

1 Running head: Differential dissolution in coccolithophores

2 **Species-specific differential dissolution morphology of selected coccolithophore**  
3 **species: an experimental study**

4 Gerald Langer<sup>1,2</sup>, Ian Probert<sup>3</sup>, Jeremy R. Young<sup>4</sup>, Patrizia Ziveri<sup>1,5,6</sup>

5 **Affiliations**

6 <sup>1</sup> Institute of Environmental Science and Technology, Universitat Autònoma de  
7 Barcelona (ICTA-UAB), Barcelona, 08193, Spain

8 <sup>2</sup> Marine Biogeochemistry, Alfred Wegener Institute, 27570 Bremerhaven, Germany

9 <sup>3</sup> Sorbonne Université/CNRS, Roscoff Culture Collection, FR2424 Station Biologique  
10 de Roscoff, 29682 Roscoff, France

11 <sup>4</sup> Earth Sciences, University College London, London WC1E 6BT, UK

12 <sup>5</sup> Catalan Institution for Research and Advanced Studies (ICREA), Barcelona, Spain

13 <sup>6</sup> BABVE Dept., Universitat Autònoma de Barcelona (ICTA-UAB), Barcelona, 08193,  
14 Spain

15

16 Corresponding author: Gerald Langer ([gerald.langer@cantab.net](mailto:gerald.langer@cantab.net),  
17 [gerald.langer@awi.de](mailto:gerald.langer@awi.de))

18

19 **500-character summary**

20 Coccolithophores are important marine CaCO<sub>3</sub> producers and their biominerals, the  
21 coccoliths, partly dissolve in the upper water column where dissolution is unexpected.  
22 Studying coccolith dissolution in field samples is hampered by a paucity of  
23 experimental studies describing dissolution morphologies. Here we fill this gap by  
24 experimentally dissolving different coccolithophores and applying our results to field  
25 samples.

26

27 **Highlights**

- 28 - Experimental studies on biogenic CaCO<sub>3</sub> dissolution provide novel insights into  
29 field sample observations and biomineralization processes
- 30 - Experimental data aid the interpretation of aberrant coccolith morphology in  
31 field samples
- 32 - In *C. braarudii* partial dissolution reveals a nanostructure in the distal shield
- 33 - The nanostructure in *C. braarudii* requires adjustments in biomineralization  
34 models

35

## 36 **Abstract**

37 Coccolith dissolution in the water column is an important process in the marine carbon  
38 cycle. Identifying dissolution in water column samples has been difficult due to a lack  
39 of experimental reference datasets showing dissolution morphologies. We conducted a  
40 laboratory CaCO<sub>3</sub> dissolution experiment to detect differential dissolution morphologies  
41 of three selected coccolithophore (abundant marine calcareous phytoplankton) species,  
42 *Coccolithus braarudii*, *Helicosphaera carteri*, and *Scyphosphaera apsteinii*. These  
43 species were selected because they are ecologically and biogeochemically important  
44 (significant contributors to CaCO<sub>3</sub> production) and have been less studied than  
45 *Gephyrocapsa*. Murooliths of *S. apsteinii* dissolve faster than lopadoliths, which in turn  
46 dissolve as fast as *H. carteri* but faster than *C. braarudii*. In *S. apsteinii* lopadoliths,  
47 dissolution rate depends on the crystallographic orientation of the crystals. Comparison  
48 with field samples shows that experimental data are helpful when interpreting field  
49 samples. For example, we identify dissolution in water and sediment samples reported  
50 in the literature. In *C. braarudii* dissolution reveals a nanostructure on the proximal side  
51 of the distal shield, an observation that has implications for coccolith biomineralization  
52 models, which do not currently account for the formation of such a structure. This  
53 nanostructure features “units” of ca 50-100 nm and resembles the nanostructure well  
54 known from extracellular calcifiers such as molluscs and foraminifera. Whether this  
55 resemblance is underpinned by a similar formation mechanism remains unknown, but  
56 we think this unlikely.

57

## 58 **1) Introduction**

59 Present anthropogenic CO<sub>2</sub> concentration changes, both atmospheric and marine,  
60 cannot be fully understood without considering marine calcium carbonate, largely  
61 produced by calcifying organisms (Broecker and Peng 1982, Morse and Mackenzie  
62 1990). These calcifying organisms influence air-sea CO<sub>2</sub> exchange in several ways, e.g.  
63 through particulate inorganic- and organic carbon production in the surface ocean but  
64 also through export of calcium carbonate to the deep ocean (Morse and Mackenzie  
65 1990). The most productive marine calcium carbonate (CaCO<sub>3</sub>) producers are pelagic  
66 organisms, with coccolithophores contributing ca. 90% of global pelagic CaCO<sub>3</sub>  
67 production (Ziveri et al., 2023) and ca. 50% of CaCO<sub>3</sub> sedimentation (Milliman 1993,  
68 Broecker and Clark 2009). Dissolution of CaCO<sub>3</sub> in the photic zone is an important  
69 process in the marine CaCO<sub>3</sub> cycle (Ziveri et al. 2023; Subhas et al. 2022; Sulpis et al.  
70 2021). The importance of dissolution for the marine C-cycle has two main aspects.  
71 Firstly, dissolution of CaCO<sub>3</sub> releases two moles of alkalinity per one mole of dissolved  
72 inorganic carbon, thereby shifting the seawater C-system towards higher pH values  
73 (Zeebe and Wolf-Gladrow, 2001). Secondly, the loss of ballast minerals reduces carbon  
74 export efficiency thereby influencing the C-cycle long-term (Klaas and Archer 2002). In  
75 addition to occurring in the open ocean photic zone, dissolution of carbonates in  
76 general, and coccoliths in particular, may also occur in sediments and coastal CO<sub>2</sub> vent  
77 sites (Honjo 1975, Ziveri et al 2014).

78 Assessing coccolith dissolution in these diverse settings can be challenging, but partial  
79 dissolution morphologies as identified in electron micrographs have proved a useful tool  
80 (e.g. Langer et al 2007, Ziveri et al 2014). Knowledge of such differential dissolution  
81 morphologies will aid interpretation of field samples, e.g. the degree of dissolution in  
82 one species will inform inferences about the degree of dissolution in other species.  
83 More fundamentally, knowledge about dissolution morphologies will enable us to  
84 accurately distinguish malformation / under-calcification from dissolution, which is not  
85 necessarily an easy task (Young 1994). Finally, dissolution might reveal informative  
86 structural features (Langer et al 2007). The main goal of our study is to provide a  
87 dissolution-morphology reference dataset which can be used to identify dissolution in  
88 water column samples. The applicability of our data to sediment samples might be more  
89 limited as discussed below. The interpretation of field samples is difficult, however,  
90 because the degree, and even the mere fact, of dissolution often need to be inferred from  
91 the micrographs alone, without precise knowledge of the physico-chemical conditions

92 leading to the observed morphology. For example, in surface sediments *Calcidiscus*  
93 *leptoporus* coccoliths (placoliths characterized by two shield-like plates connected by a  
94 central tube) lacking proximal shields have been taken as a sign of heavy dissolution  
95 (Roth and Berger 1975), which has been proposed as a proxy for dissolution in the  
96 sedimentary record (Matsuoka 1999). Only an experimental study could show that  
97 separation of the shields is the first observable dissolution feature occurring at less than  
98 8% mass loss (Langer et al 2007) revealing the “weak spot” at the proximal end of the  
99 tube (the position of the proto-coccolith ring, Young et al 2004).

100 Despite the importance of experimental studies showing graded dissolution of  
101 coccoliths, only a few such studies have been conducted (McIntyre & McIntyre 1971,  
102 Burns 1977, Kleijne 1990, Henriksen et al 2004, Langer et al 2006b, Holcová and  
103 Scheiner 2023), with a focus on *Gephyrocapsa* spp, in particular *G. huxleyi*, a widely  
104 used model species (Wheeler et al 2023). The degree of dissolution in *G. huxleyi* water  
105 column samples is difficult to assess as there are variations of progressive dissolution  
106 patterns with e.g. warm- and cold-water phenotypes (Burns 1977). The latter author  
107 pointed out that a tropical *G. huxleyi* loses the central grille in the first stages of  
108 dissolution, while a cold-water phenotype does not. Calcite removal from the long  
109 margin of the radial elements is a sign of early dissolution in the cold-water phenotype  
110 but not in a heavily calcified phenotype. These and similar observations made by Burns  
111 (1977) show that assessing the degree of dissolution in *G. huxleyi* is not an easy task  
112 and morphotype-specific assessments are required. While *G. huxleyi* is numerically the  
113 most abundant coccolithophore in present oceans, its contribution to coccolithophore  
114 CaCO<sub>3</sub> production is rivalled by some genera with larger coccoliths, such as *Calcidiscus*  
115 and *Coccolithus* (Wheeler et al 2023). The relatively recent appearance of *G. huxleyi* in  
116 the fossil record implies that this species is not applicable to deep time sediment core  
117 studies (Henderiks et al 2022). It is therefore worthwhile also studying genera with  
118 larger coccoliths and mass, biogeochemically important (Ziveri et al., 2004), and with a  
119 more extensive evolutionary history, e.g. *Coccolithus*, *Helicosphaera*, and  
120 *Scyphosphaera* (Henderiks et al 2022). The latter genera are not as abundant as *G.*  
121 *huxleyi* but play an important role in coccolithophore CaCO<sub>3</sub> production and export in  
122 modern oceans (Baumann et al., 2004; Daniels et al., 2014, 2016; Gafar et al., 2019;  
123 Ziveri et al., 2007).

124 Based largely on field sediment studies, it is accepted that some coccolith forms  
125 dissolve faster than others. While *G. huxleyi* and *Umbilicosphaera sibogae* are among  
126 the fast-dissolving placolith bearing species, *G. oceanica*, *C. leptoporus*, and *C.*  
127 *pelagicus* are comparatively slow-dissolving (McIntyre & McIntyre 1971, Berger 1973,  
128 Roth and Coulbourn 1982). These studies have not assessed how dissolution  
129 morphologies of different species relate to each other. In other words, which dissolution  
130 morphology of species x corresponds to a given dissolution morphology of species y?

131 Coccoliths contain crystals of different orientations, sizes, and shapes. A typical feature,  
132 for example, is the presence of crystals with radial c-axis orientations (R-units) and  
133 others with vertical c-axis orientations (V-units, Young et al 1992). It might therefore be  
134 hypothesized that different crystals display different structural features, not only on the  
135 micrometre but also on the nanometre scale. Some of these features might only be  
136 discernible in partially dissolved specimens.

137 In this study we selected laboratory cultures of *Coccolithus braarudii*, *Helicosphaera*  
138 *carteri*, and *Scyphosphaera apsteinii*, and performed a dissolution experiment to follow  
139 their differential dissolution morphologies by means of sequential sampling for SEM  
140 analysis. Here we analyse two important aspects of dissolution. Firstly, the selective  
141 dissolution of different species relative to each other. Secondly, the evolution of  
142 morphology of a given species with progressive dissolution. We hypothesize that  
143 dissolution morphologies will be different from malformations (Bianco et al 2025,  
144 Langer et al. 2006, Langer et al 2021, Gerecht et al 2015, Meyer et al 2020) and  
145 therefore a dissolution reference dataset will enable us to unambiguously identify  
146 dissolution in field samples. The experimental setup chosen here is ideally suited to  
147 analyse sequential dissolution morphology with nanometric resolution. This enables the  
148 identification of different dissolution stages in field samples, providing additional  
149 information over and above the mere distinction of dissolution features and  
150 malformations.

151 Experimental dissolution studies provide a good source of information on the evolution  
152 of morphology with dissolution, without confounding factors from field studies such as  
153 variance in the primary biomineralization morphology.

154

## 155 **2) Material and Methods**

156 2.1) *Culture conditions*

157 Clonal cultures of *Coccolithus braarudii* (strain RCC1198), *Scyphosphaera*  
158 *apsteinii* (strain RCC3598), and *Helicosphaera carteri* (strain RCC1323) were grown in  
159 aged (3 months), sterile-filtered (Stericup-GP Sterile Vacuum Filtration System, 0.22 µm  
160 pore size, polyethersulfone membrane, Merck) natural surface seawater sampled in the  
161 English Channel off Roscoff, France, enriched with 288 µM nitrate, 18 µM phosphate,  
162 and silicate, trace metals, and vitamins as in K/2-I ([https://roscoff-culture-](https://roscoff-culture-collection.org/medium-id/k2-i)  
163 [collection.org/medium-id/k2-i](https://roscoff-culture-collection.org/medium-id/k2-i)). All strains were obtained from the Roscoff Culture  
164 Collection (<http://www.roscoff-culture-collection.org>).

165 Cultures were grown under a 16:8 h light:dark cycle at a light intensity of  
166 50 µmol photons m<sup>-2</sup> s<sup>-1</sup> in temperature-controlled culture incubators. *Coccolithus*  
167 *braarudii* RCC1198 was grown at 15°C, while *Scyphosphaera apsteinii* RCC3598 and  
168 *Helicosphaera carteri* RCC1323 were grown at 20°C. Cells were grown in dilute batch  
169 cultures, ensuring a quasi-constant seawater carbonate system over the course of  
170 exponential growth (Hoffmann et al. 2015). Cell densities were determined by flow  
171 cytometry immediately after sampling. Cultures used in the dissolution experiment were  
172 initially checked by light and scanning electron microscopy to ensure that coccosphere  
173 morphology was normal (as observed in light microscopy) and the percentage of  
174 coccolith malformations was below 15% (as determined by SEM analysis, Langer and  
175 Bode 2011). The latter is a very low percentage of malformations in cultures (in which  
176 values up to 90% have been reported, Langer et al 2006, Langer et al 2013), enabling  
177 this study to focus on normal coccoliths and their dissolution morphologies, as opposed  
178 to the dissolution features of malformed coccoliths (Langer and Bode 2011, Langer et al  
179 2013, Langer et al 2023). We chose not to analyse the dissolution morphology of  
180 malformed coccoliths because results are intended to be applicable to field samples, in  
181 which the percentage of malformed coccoliths is typically only ca. 2% (Langer et al  
182 2006, Langer et al 2013). Analysis of the dissolution morphologies of malformed  
183 coccoliths would require a different experimental setup, with cultures displaying high  
184 proportions of malformed coccoliths. Such an approach would be interesting in itself,  
185 but does not fall within the scope of the present study (Langer et al 2006).

186 2.2) *Dissolution experiment*

187 To study differential dissolution morphologies accurately, the selected species  
188 were combined in a single 2.7L bottle (Holcová and Scheiner 2023), in which case only  
189 one calcite saturation state ( $\omega$ ) value can be selected. In pre-experiments we found  
190 that *Gephyrocapsa huxleyi* coccoliths dissolved more than 10x faster than coccoliths of  
191 *Coccolithus braarudii*, *Helicosphaera carteri*, and *Scyphosphaera apsteinii*, meaning it  
192 was not possible to include *G. huxleyi* in our experiment. The three other species, *C.*  
193 *braarudii*, *H. carteri*, and *S. apsteinii*, displayed broadly similar dissolution kinetics and  
194 were therefore suited for our purpose.

195 To start the dissolution experiment, living cells were transferred into a 2.7L bottle  
196 containing culture medium that was acidified using calculated amounts of HCl (3.29M)  
197 immediately prior to cell transfer. We used acidification to manipulate  $\omega$  calcite  
198 because it is more representative of dissolution scenarios in the field than changes in Ca  
199 concentration.  $\omega$  calcite is the saturation state of seawater with respect to calcite,  
200 with  $\omega < 1$  indicating dissolution and  $\omega > 1$  potential crystal growth. This  
201 decision is important because the manipulation of  $\omega$  calcite via acidification is  
202 more effective than via Ca concentration decrease (Hassenkam et al 2011). We chose to  
203 work with living cells, as opposed to isolated coccoliths for the following reasons.  
204 Firstly, we wanted our results to be useful for comparison with various dissolution  
205 scenarios such as whole cells in copepod and micro-grazer guts, whole cells in marine  
206 snow aggregates, whole cells in ocean acidification-affected corrosive waters. Secondly,  
207 we wanted to analyse effects of dissolution on coccospheres, as opposed to only on  
208 individual coccoliths. Thirdly, removing coccoliths from cells is not always an easy task  
209 and often requires chemical or heat treatment which might alter structural integrity and  
210 organic content (Manuela Bordiga, personal communication, 2025). Since this is a pilot  
211 study, we wanted to keep the experimental setup as straightforward as possible. Follow  
212 up studies should deal with modified setups to explore additional factors influencing  
213 dissolution patterns. The culture medium prepared using natural surface seawater  
214 sampled off Roscoff, France has a typical dissolved inorganic carbon, DIC, of ca 2000  
215  $\mu\text{mol kg}^{-1}$  (Johnson et al 2022). We used this value for DIC and measured pH (NBS) =  
216 6.44 to calculate  $\omega$  calcite = 0.033 using the program CO2SYS (Pierrot et al 2011).  
217 The calculated value for  $\omega$  calcite (0.033) was therefore approximate. However,  
218 DIC variability of natural surface seawater sampled off Roscoff, France is low, therefore  
219 introducing only a negligible inaccuracy in calculated  $\omega$  calcite in the context of

220 the present study, i.e. an error of  $\pm 0.005$  is expected (Johnson et al 2022). The present  
221 study was not designed to analyse dissolution kinetics precisely (such as in Subhas et al  
222 2018), meaning an approximate determination of the carbonate system is sufficient. We  
223 used a Cyberscan 500 pH meter (Eutech Instruments, UK) equipped with a Mettler  
224 Toledo InLab 413/ID67 electrode to determine pH on the NBS scale.

225 Experimental dissolution over a very short space of time (on the order of seconds as in  
226 Yang et al 2021) only allows for comparatively low-resolution light micrographs that  
227 would have been insufficient for our purpose. The advantage of a short experiment  
228 duration, however, is that DIC uptake and gas exchange with the atmosphere, and  
229 therefore carbonate system variability, is negligible. Our dissolution experiment,  
230 conducted over a duration of 11 hours, was carried out in the dark at 4°C to ensure that  
231 cellular metabolism (including photosynthesis and coccolith production) was severely  
232 restricted over the course of the experiment. Cell densities were 711 cells/mL for *C.*  
233 *braarudii*, 665 cells/mL for *H. carteri*, and 586 cells/mL for *S. apsteinii*. The resultant  
234 low overall cell density of 1963 cells/mL contributed to ensuring a quasi-constant  
235 carbonate system over the course of the experiment (Langer et al 2006, Langer and  
236 Bode 2011, Hoffmann et al 2015). Physico-chemical conditions over the course of the  
237 experiment were additionally homogenized by regular mixing, i.e. keeping the cells in  
238 suspension. No aggregation of cells occurred and no sedimentation of cells or coccoliths  
239 took place. The pH did rise by ca 0.1 over the course of the experiment, but this  
240 corresponds to an increase in omega calcite of only ca. 0.005, i.e. the same magnitude as  
241 the minor uncertainty introduced by our choice of DIC value (see above).

242 After the dissolution experiment was completed, cells were transferred into normal  
243 culture conditions as specified above. All three species, *C. braarudii*, *H. carteri*, and *S.*  
244 *apsteinii*, resumed cell division and coccolith production as confirmed by optical  
245 inspection using light microscopy. We did not quantify coccolith morphology in re-  
246 calcifying cells, but noted that initially coccoliths seemed to display more  
247 malformations than prior to the dissolution experiment. This assessment is based on an  
248 informal analysis by means of light microscopy; no images were taken.

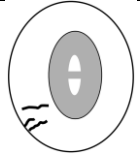
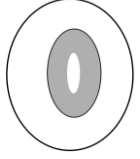
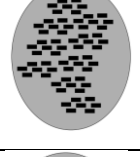
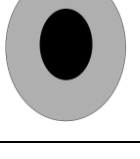
249 Multiple (15) sequential samples for detailed morphological analysis were taken over  
250 the 11 hour duration of the experiment. Samples for SEM analysis were filtered onto  
251 polycarbonate filters (0.8  $\mu\text{m}$  pore-size), dried in a drying cabinet at 50°C for 24 h, then  
252 sputter-coated with gold-palladium using a Cressington 108 sputter coater (Cressington

253 Scientific Instruments, Watford, UK). Imaging was performed with a Phenom Pro  
 254 desktop SEM at the Station Biologique de Roscoff, France, and an EI SEM Zeiss Merlin  
 255 at UAB, Barcelona, Spain. All the morphological features described in this study are  
 256 discernible using the Phenom Pro desktop SEM. We used the Zeiss Merlin FE-SEM  
 257 only to produce images showing the nanostructure on the proximal side of the distal  
 258 shield of *C. braarudii* because the latter microscope has a higher resolution. This  
 259 nanostructure, however, was discovered using the Phenom Pro desktop SEM. An  
 260 average of ~350 coccoliths was analysed per sample (Langer and Benner 2009). To  
 261 describe dissolution morphologies, we selected conspicuous features that could be  
 262 easily followed over the course of the experiment to ensure robust results and to  
 263 facilitate application to field samples. In *C. braarudii* and *H. carteri* we analysed  
 264 dissolution features of coccospheres in addition to dissolution features of coccoliths. In  
 265 *S. apsteinii* only dissolution features of coccoliths were analysed because coccospheres  
 266 in this species lack the mechanical stability needed to consistently withstand the  
 267 mechanical forces experienced in SEM preparation (Langer et al 2023). The following  
 268 morphological features were used to describe dissolution. In *C. braarudii*: 1) etching of  
 269 the inner tube, 2) etching of the distal shield, 3) central area bar missing, 4) coccoliths  
 270 broken, 5) gaps in coccospheres, 6) coccospheres collapsed, 7) nanostructure visible (on  
 271 proximal side of distal shield). In *H. carteri*: 1) etching, 2) coccoliths broken, 3)  
 272 coccospheres collapsed. In *S. apsteinii* lopadoliths: 1) etching of base, 2) etching of  
 273 barrel, 3) rim serrated, 4) lopadoliths broken, 5) isolated lopadolith V units. In *S.*  
 274 *apsteinii* muraliths: 1) centre missing, 2) etching, 3) muraliths broken. Scanning  
 275 electron micrographs of all of these features are shown in Figs 1-5. The most important  
 276 dissolution features for practical purposes are summarised in Table 1.

277 Table 1. Summary of important dissolution features.

278

| coccolith           | dissolution feature   | sketch  |
|---------------------|-----------------------|---|
| <i>C. braarudii</i> | etching of inner tube |  |

|                                    |                          |   |
|------------------------------------|--------------------------|---|
| <i>C. braarudii</i>                | etching of distal shield |    |
| <i>C. braarudii</i>                | central area bar missing |    |
| <i>H. carteri</i>                  | etching                  |    |
| <i>S. apsteinii</i><br>lopadoliths | etching of barrel        |    |
| <i>S. apsteinii</i><br>lopadoliths | serrated rim             |   |
| <i>S. apsteinii</i><br>muroliths   | etching                  |  |
| <i>S. apsteinii</i><br>muroliths   | centre missing           |  |

279

280

### 281 3) Results and Discussion

#### 282 3.1) Differential dissolution: general observations

283 We subjected living cells of three common coccolithophore species, namely  
 284 *Coccolithus braarudii*, *Helicosphaera carteri*, and *Scyphosphaera apsteinii*, to seawater  
 285 undersaturated with respect to calcite, i.e. omega calcite ca. 0.033 (see Methods). The  
 286 duration of the experiment was 11 hours, at the end of which only a few isolated distal

287 shield elements of *C. braarudii* remained (Fig 6). Our observation that *C. braarudii* is  
288 more dissolution resistant than *H. carteri* tallies well with conclusions drawn from  
289 studying Atlantic Ocean floor sediments (Berger 1973). Information on *S. apsteinii* in  
290 differential dissolution studies is rare, with this species either only mentioned but not  
291 discussed or not mentioned at all (McIntyre & McIntyre 1971, Berger 1973, Roth and  
292 Coulbourn 1982). From our data we conclude that *S. apsteinii* lopadoliths display  
293 dissolution kinetics similar to *H. carteri*, while *S. apsteinii* muraliths dissolve faster. In  
294 *S. apsteinii*, R-units, which are smaller and radially oriented, dissolve conspicuously  
295 faster than the larger, vertically oriented V-units (Figs 6, 7, see also Drescher et al  
296 2012). Since lopadoliths contain calcite only, as opposed to e.g. aragonite (Walker et al  
297 2024), the latter observation illustrates that differential dissolution kinetics of biogenic  
298 calcium carbonate cannot be inferred from the polymorph only (Langer and Ziveri  
299 2025). Both etching and broken coccoliths appear simultaneously in *S. apsteinii*  
300 lopadoliths and *H. carteri* (Figs 6, 7). In *C. braarudii* etching of the inner tube occurs  
301 simultaneously with etching in *H. carteri* and *S. apsteinii*, but etching of the *C.*  
302 *braarudii* distal shield appears later, possibly because the latter features the largest  
303 crystals (Figs 6, 7). Relatively slow dissolution of the distal shield compared to the  
304 tube/central area was also observed in *C. leptoporus* and might be a general feature of  
305 Coccolithales placoliths (Langer et al 2007).

### 306 3.2) Comparison with field samples

307 Identification of dissolution in field samples:

308 As noted in the introduction coccolith dissolution in the water column is being  
309 highlighted as a key process, greatly affecting the export production of coccolith  $\text{CaCO}_3$   
310 to the bottom sediment. Our experimental results on the sequence of dissolution stages  
311 might usefully be applied to study of field samples in order to analyse and track water  
312 column dissolution. As a proof of concept we show here (Fig 8) images of *Coccolithus*  
313 *braarudii* and *Helicosphaera carteri* coccoliths from sediment trap samples and of  
314 coccoliths from water column samples, in both cases showing dissolution features  
315 directly comparable to those we observed experimentally. It is also noteworthy that the  
316 nanostructure seen in the experimental samples is visible in the field samples (Fig 8)  
317 showing that it is not an experimental artefact. Comparable dissolution features have  
318 also been illustrated in the literature, for example by Cubillos et al (2012) and Kleijne  
319 (1990), although in some cases they have been ascribed to malformation.

320 It is striking that in the three species studied here dissolution morphologies are clearly  
321 different from malformations. The latter do not resemble etching as described here (Figs  
322 1-5). This is remarkable considering that it has typically been difficult to distinguish  
323 dissolution from malformation, and even fracture, in *G. huxleyi* (McIntyre & McIntyre  
324 1971, Burns 1977, Kleijne 1990, Holcová and Scheiner 2023, Young 1994, Langer et al  
325 2006b, Langer and Benner 2009, Langer et al 2011). These difficulties in identifying  
326 dissolution morphology in *G. huxleyi* are particularly conspicuous in morpho-type B/C,  
327 but are clearly noticeable in type A as well (own observations, unpublished). It might be  
328 speculated that dissolution is easier to identify in type R because the latter features  
329 fused distal shield elements which makes the overall morphology more similar to the  
330 one of the species studied here. This conjecture is supported by *G. huxleyi* morphotype-  
331 specific dissolution morphologies described in water column samples (Burns 1977). It  
332 will be worthwhile studying different *G. huxleyi* morphotypes in greater detail. Species-  
333 specific dissolution features such as the serrated rim in *S. apsteinii* lopadoliths are also  
334 dissimilar to malformations such as type R (Langer et al 2021, Langer et al 2023). The  
335 nanostructure on the proximal side of the distal shield of *C. braarudii* is hardly visible  
336 in normal as well as malformed coccoliths, whereas it is clearly visible in partially  
337 dissolved coccoliths. In *C. braarudii* a concentric hole sometimes appears in malformed  
338 coccoliths (Langer et al 2021). This hole is clearly different from etch pits. A typical  
339 feature of more severe malformations in placolith bearing species is the distorted  
340 architecture of the shields (Bianco et al 2025, Langer et al 2006, Langer and Benner  
341 2009, Langer et al 2011, Langer and Bode 2011, Langer et al 2012, Langer et al 2013,  
342 Langer et al 2021, Langer et al 2023, Kottmeier et al 2022, Gerech et al 2015, Milner et  
343 al 2016, Johnson et al 2022) which does not occur as a result of dissolution.

344 Do the conditions under which dissolution occurs influence dissolution  
345 morphologies?

346 As a caveat we will say that dissolution morphologies might well depend on the  
347 conditions under which dissolution occurs. For example, the presence or absence of an  
348 organic coating around coccoliths results in slightly different dissolution morphologies  
349 as seen in high resolution AFM imaging (Henriksen et al 2004). Since we did not  
350 remove the organic coating, our results should be best applicable to water samples (with  
351 organic coating) as opposed to sediment samples (in which the organic coating might be  
352 degraded). That said, the organic coating of coccoliths can still slow down dissolution

353 after 70Ma in the sediment (Sand et al 2014). Whether dissolution morphologies of  
354 these ancient coccoliths would be similar to those of cultured specimens remains to be  
355 tested. A good candidate would be *C. pelagicus* because it first appeared in the fossil  
356 record more than 60 Ma (Henderiks et al 2022). Another aspect to consider is the way  
357 undersaturation is achieved. Dissolution kinetics in low-Ca solutions are different from  
358 those in low-pH solutions (Hassenkam et al 2011). It is an open question whether  
359 dissolution morphologies would differ too. In addition, pressure-driven undersaturation  
360 might be relevant for deep-sea sediment samples. All of these issues are amenable to  
361 experimental testing and should be the focus of future studies.

### 362 3.3) Structural integrity of the coccosphere

363 An interesting difference between *C. leptoporus* (Langer et al 2007) on the one  
364 hand and *C. braarudii* / *H. carteri* (this study) on the other hand is the structural  
365 integrity of coccospheres under dissolution. The earliest feature of dissolution in *C.*  
366 *leptoporus* dissolved at an omega calcite of 0.5, is the separation of the shields resulting  
367 in coccosphere collapse (Langer et al 2007). By contrast, in *C. braarudii* and *H. carteri*  
368 the earliest dissolution feature is etching leaving the coccospheres intact. Only when  
369 coccoliths break due to more pronounced etching do coccospheres collapse in these  
370 species (Fig 7). This means that living *C. leptoporus* cells are more vulnerable to  
371 dissolution than *C. braarudii* / *H. carteri* because all three species need a coccosphere  
372 to live (Walker et al 2018a, Bianco et al., 2025). While a coccosphere comprised of  
373 coccoliths produced by the very cell itself is essential for survival in monospecific  
374 cultures of these species, mixed-species coccospheres in natural assemblages indicate  
375 that coccosphere integrity can be re-established or modified through incorporation of  
376 foreign coccoliths (Johns et al 2023). This might mean that a coccosphere compromised  
377 through dissolution or malformation might be repaired by incorporating foreign  
378 coccoliths. The protective efficacy of such hybrid coccospheres remains to be tested  
379 experimentally. However, the vulnerability sequence described above differs from what  
380 would be expected based on species specific coccolith solubility as inferred from  
381 sediment samples, which do not suggest that *C. leptoporus* is more vulnerable than *H.*  
382 *carteri* (Berger 1973). Note that we cannot be entirely sure that *C. leptoporus* coccoliths  
383 would break faster than *H. carteri* coccoliths when subjected to the same omega calcite  
384 because the *C. leptoporus* experiment was conducted at an omega calcite of 0.5 (Langer  
385 et al 2007) as opposed to the ca 0.033 used here. Nevertheless, considering the very

386 early appearance of separated shields in *C. leptoporus* (Langer et al 2007) and the  
387 comparatively late appearance of broken coccoliths in *H. carteri*, it is highly likely that  
388 coccosphere collapse in *C. leptoporus* would occur earlier than in *H. carteri* (at a given  
389 omega calcite). Although bulk surface waters in most parts of the global ocean are  
390 currently supersaturated with respect to calcite, ongoing ocean acidification drives the  
391 calcite saturation state towards undersaturation which will be reached in some areas,  
392 e.g. the Southern Ocean, around the year 2100, posing a threat to calcifying organisms  
393 including coccolithophores (Langer and Ziveri 2025). Please note that most surface  
394 waters will remain supersaturated with respect to calcite, so that our results are most  
395 directly relevant to locally undersaturated conditions (e.g. upwelling regions, eddies,  
396 sea-ice melt, or pore waters). Regardless of the actual threat posed by corrosive waters  
397 to living coccolithophores, the argument we are making here centres on relative  
398 vulnerability of different species in case of calcite undersaturation.

#### 399 3.4) *A nanostructure in C. braarudii biomineral*

400 A nanostructure on the proximal side of the distal shield in *C. braarudii* became  
401 visible 3 hours into the experiment (Fig. 6). The individual “units” of this nanostructure  
402 are ca. 50-100 nm in diameter. The distal side of the distal shield does not show this  
403 nanostructure. Differences between the proximal and distal sides of the distal shield  
404 have previously been reported (Henriksen et al 2004, Young et al 2004). Whereas the  
405 distal side of the distal shield consists of crystallographic a-faces, the proximal side  
406 seems to be more profoundly regulated by the cell and does not show crystallographic  
407 faces (Young et al 2004). The nanostructure shown here is what was described as  
408 “tuberculate surface” by Henriksen et al. (2004). The latter authors conclude that the  
409 tubercles are part of the calcite structure. We confirm this conclusion which is illustrated  
410 particularly well by a side view of these tubercles (Fig. 3D). We can only speculate what  
411 effect this nanostructure might have on the dissolution resistance / susceptibility of the  
412 distal shield elements. Considering that the distal shield elements of *C. braarudii* are the  
413 only coccolith parts of all three species that are still present at the end of the experiment  
414 (Fig. 6), it seems clear that they are comparatively dissolution resistant. Whether this  
415 resistance stems from the nanostructure or some other feature remains an open question  
416 but it is fair to say that the nanostructure does not make coccolith crystals highly  
417 susceptible to dissolution. The importance of micro- and nanostructures in differential  
418 dissolution behaviour of various biominerals has been recently highlighted in the

419 context of vulnerability to ocean acidification (Langer and Ziveri 2025). It is  
420 conceivable that the nanostructure in *C. braarudii* slows down etching and / or provides  
421 structural reinforcement. This scenario would be plausible if the nanostructure was an  
422 organo-mineral composite structure as opposed to being composed of calcite only  
423 (Walker and Langer 2021). A nanostructure of similar size in CaCO<sub>3</sub> biominerals is  
424 widespread in extracellular calcifiers, where it is a central indicator of a layered growth  
425 mechanism featuring particle accretion which is believed to be non-operative in  
426 coccolithophores (Kadan et al 2021, Walker and Langer 2021). It remains, however, an  
427 open question whether the nanostructure in *C. braarudii* is similar to that in  
428 extracellular calcifiers i.e. whether it is also an organo-mineral composite structure  
429 (Walker and Langer 2021). This question is pertinent to coccolithophore  
430 biomineralization because an extracellular-like nanostructure in coccoliths would call  
431 into question widely held views about crystallization of coccolith crystals (Walker and  
432 Langer 2021). However, even if the tuberculate nanostructure in *C. braarudii* should  
433 turn out to be extracellular-like, it would still be unclear how it is possible that the distal  
434 side of the distal shield is different, i.e. shows crystallographic a-faces and no  
435 nanostructure. The standard biomineralization model explaining the nanostructure in  
436 extracellular calcifiers cannot account for the difference between the two sides of the  
437 distal shield in *C. braarudii*, and neither can the standard model of coccolith  
438 biomineralization (Young et al 2004, Walker and Langer 2021). This difference between  
439 the proximal and the distal side of the distal shield shows how finely tuned  
440 morphogenesis in *C. braarudii* is. We can only speculate how this fine tuning is  
441 achieved, but the composition of the organic coating might play a role. The composition  
442 of coccolith associated polysaccharides is known to be species specific, but we  
443 speculate that it might also be site specific within the coccolith vesicle (Walker et al  
444 2018b).

#### 445 **4) Conclusions**

446 In summary, our results show that dissolution experiments complement field studies and  
447 contribute to a deeper understanding of both coccolith structure and the ecological  
448 impact of seawater undersaturation with respect to calcite. We conclude that

449 1) the most dissolution-resistant species is *C. braarudii*, followed by *H. carteri* and *S.*  
450 *apsteinii*;

451 2) structural integrity of the coccosphere under dissolution is highest in *C. braarudii*,  
452 followed by *H. carteri* and *S. apsteinii*, with *C. leptoporus* probably showing the  
453 weakest coccosphere;

454 3) we identify dissolution in published field data where it was not recognised;

455 4) lopadolith R-units dissolve faster than V-units, illustrating that different  
456 microstructures in the same coccolith have different dissolution kinetics despite  
457 containing the same mineral;

458 5) the nanostructure in the distal shield of *C. braarudii* points to a fine-tuning in  
459 coccolith morphogenesis that is not accounted for by our current model of coccolith  
460 biomineralization.

461

#### 462 **Acknowledgements**

463 No acknowledgements at this stage.

#### 464 **Funding:**

465 Generalitat de Catalunya (MERS, 2021 SGR00640), Spanish Ministry of Science and  
466 Innovation (CEX2019-000940-M), and BIOCAL project (PID2020-113526RB-I00,  
467 Spanish Ministry of Science and Innovation). DFG project BONITOS 541693727.

#### 468 **Competing interests**

469 The authors declare no conflict of interests.

#### 470 **Author contributions**

471 GL: conception, experiments, analysis, writing, IP: experiments, writing, JRY: analysis,  
472 field samples, writing, PZ: writing.

#### 473 **Data availability**

474 The data will be archived at PANGAEA and the DOI will be added in the final version.

475

#### 476 **References**

477 Baumann, K.-H., Böckel, B., and Frenz, M.: Coccolith contribution to South Atlantic  
478 carbonate sedimentation, in: Coccolithophores, edited by: Thierstein, H. R. and Young,  
479 J. R., Springer Berlin Heidelberg, Berlin, Heidelberg, 367–402,  
480 [https://doi.org/10.1007/978-3-662-06278-4\\_14](https://doi.org/10.1007/978-3-662-06278-4_14), 2004.

481 Berger WH (1973) Deep-sea carbonates: evidence for a coccolith lysocline. *Deep-Sea*  
482 *Res* 20:917–921

483 Bianco, S., Bordiga, M., Langer, G., Ziveri, P., Cerino, F., Di Giulio, A., and Lupi, C.  
484 (2025) Low sensitivity of a heavily calcified coccolithophore under increasing CO<sub>2</sub>: the  
485 case study of *Helicosphaera carteri*, *Biogeosciences*, 22, 1821–1837,  
486 <https://doi.org/10.5194/bg-22-1821-2025>.

487 Broecker, W. & Clark, E. Ratio of coccolith CaCO<sub>3</sub> to foraminifera CaCO<sub>3</sub> in late  
488 Holocene deep sea sediments. *Paleoceanogr.* 24, PA3205 (2009).

489 Broecker, W. S. & Peng, T.-H. *Tracers in the Sea*. 690 (Lamont-Doherty Geological  
490 Observatory, Columbia University, 1982)

491 Broerse, A.T.C., Ziveri, P., Honjo, S., (2000) Coccolithophore (CaCO<sub>3</sub>) flux in the Sea  
492 of Okhotsk: seasonality, settling and alteration processes *Marine Micropaleontology*, 39  
493 (1-4): 179-200.

494 Burns, D. A. (1977). Phenotypes and dissolution morphotypes of the genus  
495 *Gephyrocapsa* Kamptner and *Emiliana huxleyi* (Lohmann). *New Zealand Journal of*  
496 *Geology and Geophysics*, 20(1), 143-155.

497 Cubillos, J.C., Henderiks, J., Beaufort, L., Howard, W.R., & Hallegraeff, G.M. (2012).  
498 Reconstructing calcification in ancient coccolithophores: Individual coccolith weight  
499 and morphology of *Coccolithus pelagicus* (sensu lato). *Marine Micropaleontology*, 92,  
500 29-39.

501 Daniels, C., Poulton, A., Young, J., Esposito, M., Humphreys, M., Ribas-Ribas, M.,  
502 Tynan, E., and Tyrrell, T.: Species-specific calcite production reveals *Coccolithus*  
503 *pelagicus* as the key calcifier in the Arctic Ocean, *Mar. Ecol. Prog. Ser.*, 555, 29–47,  
504 <https://doi.org/10.3354/meps11820>, 2016.

505 Daniels, C. J., Sheward, R. M., and Poulton, A. J.: Biogeochemical implications of  
506 comparative growth rates of *Emiliana huxleyi* and *Coccolithus* species,  
507 *Biogeosciences*, 11, 6915–6925, <https://doi.org/10.5194/bg-11-6915-2014>, 2014.

508 Drescher B, Dillaman RM, Taylor AR. (2012) Coccolithogenesis In *Scyphosphaera*  
509 *apsteinii* (Prymnesiophyceae). *J Phycol.* 2012 Dec;48(6):1343-61. doi: 10.1111/j.1529-  
510 8817.2012.01227.x. Epub 2012 Sep 17. PMID: 27009987.

511 Gafar, N. A., Eyre, B. D., and Schulz, K. G.: Particulate inorganic to organic carbon  
512 production as a predictor for coccolithophorid sensitivity to ongoing ocean acidification,  
513 *Limnol. Oceanogr. Letters*, 4, 62–70, <https://doi.org/10.1002/lol2.10105>, 2019

514 Gerecht AC, Supraha L, Edvardsen B, Langer G, Henderiks J. 2015. Phosphorus  
515 availability modifies carbon production in *Coccolithus pelagicus* (Haptophyta). *Journal*  
516 *of Experimental Marine Biology and Ecology* 472: 24–31.

517 Gupta, .M., Banerjee, R. & Mergulhao, L. On the nature of the calcareous substrate of  
518 a ferromanganese crust from the Vityaz Fracture Zone, Central Indian Ridge: (2002).  
519 inferences on paleoceanography. *Geo-Mar Lett* 22, 12–18 (2002).  
520 <https://doi.org/10.1007/s00367-002-0091-0>

521 Hassenkam, T., Johnsson, A. M. S., Bechgaard, K., & Stipp, S. L. S. (2011). Tracking  
522 single coccolith dissolution with picogram resolution and implications for CO<sub>2</sub>  
523 sequestration and ocean acidification. *Proceedings of the National Academy of Sciences*  
524 *of the United States of America*, 108, 8571-8576.

525 Henderiks, J., Sturm, D., Šupraha, L., & Langer, G. (2022). Evolutionary Rates in the  
526 Haptophyta: Exploring Molecular and Phenotypic Diversity. *Journal of Marine Science*  
527 *and Engineering*, 10(6), 798. <https://doi.org/10.3390/jmse10060798>

528 Henriksen, K., Young, J. R., Bown, P. R., & Stipp, S. L. S. (2004). Coccolith  
529 biomineralisation studied with atomic force microscopy. *Palaeontology*, 47(3), 725-743.

530 Hoffmann, R., Kirchlechner, C., Langer, G., Wochnik, A. S., Griesshaber, E., Schmahl,  
531 W. W., and Scheu, C. (2015) Insight into *Emiliana huxleyi* coccospheres by focused ion  
532 beam sectioning, *Biogeosciences*, 12, 825–834, <https://doi.org/10.5194/bg-12-825-2015>,  
533 2015.

534 Holcová K, Scheiner F. (2023). An experimental study on post-mortem dissolution and  
535 overgrowth processes affecting coccolith assemblages: A rapid and complex process.  
536 *Geobiology*. 2023 Mar;21(2):193-209. doi: 10.1111/gbi.12528. Epub 2022 Oct 11.  
537 PMID: 36218003.

538 Honjo,S. 1975. "DISSOLUTION OF SUSPENDED COCCOLITHS IN THE DEEP-  
539 SEA WATER COLUMN AND SEDIMENTATION OF COCCOLITH OOZE",  
540 *Dissolution of Deep-sea Carbonates*, William V. Sliter, Allan W. H. Bé, Wolfgang H.  
541 Berger

542 Johns, CT et al. Adsorptive exchange of coccolith biominerals facilitates viral infection.  
543 *Sci. Adv.*9, eadc8728(2023). DOI:10.1126/sciadv.adc8728

544 Johnson, R., Langer, G., Rossi, S., Probert, I., Mammone, M., & Ziveri, P. (2022).  
545 Nutritional response of a coccolithophore to changing pH and temperature. *Limnology*  
546 *and Oceanography*, 67(10), 2309-2324.

547 Kadan Y, Tollervey F, Varsano N, Mahamid J, Gal A. (2021) Intracellular nanoscale  
548 architecture as a master regulator of calcium carbonate crystallization in marine  
549 microalgae. *Proc Natl Acad Sci U S A*. 2021 Nov 16;118(46):e2025670118. doi:  
550 10.1073/pnas.2025670118. PMID: 34772804; PMCID: PMC8694050.

551 Kleijne, A. (1990). Distribution and malformation of extant calcareous nannoplankton  
552 in the Indonesian Seas. *Marine Micropaleontology*, 16(3-4), 293-316.

553 Langer, G. & Benner, I. (2009) Effect of elevated nitrate concentration on calcification  
554 in *Emiliana huxleyi*. *J. Nannoplankton Res.* 30: 77–80.

555 Langer, G., & Bode, M. (2011). CO<sub>2</sub> mediation of adverse effects of seawater  
556 acidification in *Calcidiscus leptoporus*. *Geochemistry, Geophysics, Geosystems*, 12(5).  
557 <https://doi.org/10.1029/2010GC003393>

558 Langer, G., Geisen, M., Baumann, K. H., Kläs, J., Riebesell, U., Thoms, S., & Young, J.  
559 R. (2006). Species-specific responses of calcifying algae to changing seawater  
560 carbonate chemistry. *Geochemistry, geophysics, geosystems*, 7(9).

561 Langer, G., Gussone, N., Nehrke, G., Riebesell, U., Eisenhauer, A., Kuhnert, H., Rost,  
562 B., Trimborn, S., & Thoms, S. (2006b). Coccolith strontium to calcium ratios in  
563 *Emiliana huxleyi*: The dependence on seawater strontium and calcium concentrations.

564 Limnology and Oceanography, 51(1 I), 310-320.  
565 <https://doi.org/10.4319/lo.2006.51.1.0310>

566 Langer, G., Nehrke, G., & Jansen, S. (2007). Dissolution of *Calcidiscus leptoporus*  
567 coccoliths in copepod guts? A morphological study. *Marine Ecology Progress Series*,  
568 331, 139-146.

569 Langer, G., Oetjen, K., Brenneis, T. (2013). On culture artefacts in coccolith  
570 morphology. *Helgoland Marine Research*, 67(2), 359-369.  
571 <https://doi.org/10.1007/s10152-012-0328-x>

572 Langer G, Taylor AR, Walker CE, Meyer EM, Ben Joseph O, Gal A, Harper GM,  
573 Probert I, Brownlee C, Wheeler GL. Role of silicon in the development of complex  
574 crystal shapes in coccolithophores. *New Phytol.* 2021 Sep;231(5):1845-1857. doi:  
575 10.1111/nph.17230. Epub 2021 Mar 9. PMID: 33483994.

576 Langer G, Probert I, Cox MB, Taylor A, Harper GM, Brownlee C, Wheeler G. (2023)  
577 The Effect of cytoskeleton inhibitors on coccolith morphology in *Coccolithus braarudii*  
578 and *Scyphosphaera apsteinii*. *J Phycol.* 2023 Feb;59(1):87-96. doi: 10.1111/jpy.13303.  
579 Epub 2022 Dec 24. PMID: 36380706.

580 Langer G. & Ziveri P. (2025) Vulnerability to ocean acidification of marine calcifying  
581 organisms cannot be predicted from the mineral type in their shells. *Limnology and*  
582 *Oceanography Letters* 10(4): 448-452. <https://doi.org/10.1002/lol2.70020>

583 Matsuoka, H. (1990) A new method to evaluate dissolution of CaCO<sub>3</sub> in the deep-sea  
584 sediments. *Trans. Proc. Paleont. Soc. Jpn.*, 157, 430-434

585 McIntyre A, McIntyre R (1971) Coccolith concentration and differential solution in  
586 oceanic sediments. In: Funnel BM, Riedel WR (eds) *The micropaleontology of oceans*.  
587 Cambridge University Press, Cambridge, p 253–2610

588 Meyer, Erin M., Langer, Gerald, Brownlee, Colin, Wheeler, Glen L. and Taylor, Alison  
589 R. 2020 Sr in coccoliths of *Scyphosphaera apsteinii*: Partitioning behavior and role in  
590 coccolith morphogenesis. *Geochimica et Cosmochimica Acta*, 285. 41-54.  
591 10.1016/j.gca.2020.06.023

592 Milliman, J. D. Production and accumulation of calcium carbonate in the ocean: budget  
593 of a nonsteady state. *Glob. Biogeochemical Cycles* 7, 927–957 (1993).

594 Morse, J. W. & Mackenzie, F. T. *Geochemistry of sedimentary carbonates*. (Elsevier,  
595 1990).

596 Pierrot, D., D. Wallace, E. Lewis, R. Wallace, and W. Wallace. (2011) MS Excel  
597 Program Developed for CO<sub>2</sub> System Calculations. ORNL Environmental Sciences  
598 Division. doi:10.3334/CDIAC/otg

599 Roth PH, Berger WH (1975) Distribution and dissolution of coccoliths in the south and  
600 central Pacific. In: Sliter WV, Be AWH, Berger WH (eds) CaCO<sub>3</sub> dissolution in the  
601 deep sea. Cushman Foundation for Foraminiferal Research, Santa Barbara, CA, p 87–  
602 113

603 Roth, P. H., & Coulbourn, W. T. (1982). Floral and solution patterns of coccoliths in  
604 surface sediments of the North Pacific. *Marine Micropaleontology*, 7(1), 1–52.  
605 doi:10.1016/0377-8398(82)90014-7

606 Sand, K., Pedersen, C., Sjoberg, S., Nielsen, J., Makovicky, E., and Stipp, S. (2014).  
607 Biomineralization: long-term effectiveness of polysaccharides on the growth and  
608 dissolution of calcite. *Cryst. Growth Des.* 14, 5486–5494. doi: 10.1021/cg5006743

609 Subhas, A. V., Rollins, N. E., Berelson, W. M., Erez, J., Ziveri, P., Langer, G., & Adkins,  
610 J. F. (2018). The dissolution behavior of biogenic calcites in seawater and a possible  
611 role for magnesium and organic carbon. *Marine Chemistry*, 205, 100-112.  
612 <https://doi.org/10.1016/j.marchem.2018.08.001>

613 Subhas, A. V., Dong, S., Naviaux, J. D., Rollins, N. E., Ziveri, P., Gray, W., Rae, J. W.  
614 B., Liu, X., Byrne, R. H., Chen, S., Moore, C., Martell-Bonet, L., Steiner, Z., Antler, G.,  
615 Hu, H., Lunstrum, A., Hou, Y., Kemnitz, N., Stutsman, J., ... Adkins, J. F. (2022).  
616 Shallow Calcium Carbonate Cycling in the North Pacific Ocean. *Global*  
617 *Biogeochemical Cycles*, 36(5). <https://doi.org/10.1029/2022GB007388>

618 Sulpis, O., Jeansson, E., Dinauer, A., Lauvset, S. K., & Middelburg, J. J. (2021).  
619 Calcium carbonate dissolution patterns in the ocean. *Nature Geoscience*, 14(6), 423–  
620 428. <https://doi.org/10.1038/s41561-021-00743-y>

621 Walker JM, Langer G. (2021) Coccolith crystals: Pure calcite or organic-mineral  
622 composite structures? *Acta Biomater.* 2021 Apr 15;125:83-89. doi:  
623 10.1016/j.actbio.2021.02.025. Epub 2021 Feb 22. PMID: 33631395.

624 Walker JM, Greene HJM, Moazzam Y, Quinn PD, Parker JE, Langer G. (2024) An  
625 uneven distribution of strontium in the coccolithophore *Scyphosphaera apsteinii*  
626 revealed by nanoscale X-ray fluorescence tomography. *Environ Sci Process Impacts*.  
627 2024 Jun 19;26(6):966-974. doi: 10.1039/d3em00509g. PMID: 38354057.

628 Walker CE, Taylor AR, Langer G, Durak GM, Heath S, Probert I, Tyrrell T, Brownlee  
629 C, Wheeler GL. (2018a) The requirement for calcification differs between ecologically  
630 important coccolithophore species. *New Phytol*. 2018 Oct;220(1):147-162. doi:  
631 10.1111/nph.15272. Epub 2018 Jun 19. PMID: 29916209; PMCID: PMC6175242.

632 Walker, Charlotte E., Heath, Sarah, Salmon, Deborah L., Smirnoff, Nicholas, Langer,  
633 Gerald, Taylor, Alison R., Brownlee, Colin and Wheeler, Glen L. (2018b) An  
634 extracellular polysaccharide-rich organic layer contributes to organization of the  
635 coccosphere in coccolithophores. *Frontiers in Marine Science*, 5 (AUG), [306].  
636 (doi:10.3389/fmars.2018.00306).

637 Wheeler GL, Sturm D, Langer G. (2023) *Gephyrocapsa huxleyi* (*Emiliana huxleyi*) as a  
638 model system for coccolithophore biology. *J Phycol*. 2023 Dec;59(6):1123-1129. doi:  
639 10.1111/jpy.13404. Epub 2023 Nov 20. PMID: 37983837.

640 Yang M, Batchelor-McAuley C, Barton S, Rickaby REM, Bouman HA, Compton RG.  
641 (2021) Opto-Electrochemical Dissolution Reveals Coccolith Calcium Carbonate  
642 Content. *Angew Chem Int Ed Engl*. 2021 Sep 13;60(38):20999-21006. doi:  
643 10.1002/anie.202108435. Epub 2021 Aug 15. PMID: 34288323; PMCID:  
644 PMC8518593.

645 Young, J. R. (1994). Variation in *Emiliana huxleyi* coccolith morphology in samples  
646 from the Norwegian EHUX experiment, 1992. *Sarsia*. 79(4): 417-425.

647 Young, J. R. (2008). *Scyphosphaera porosa* Kamptner 1967 rediscovered in the  
648 plankton. *Journal of Nanoplankton Research*. 30(1): 35-38

649 Young, J. R., Henriksen, K., & Probert, I. (2004). Structure and morphogenesis of the  
650 coccoliths of the CODENET species. In *Coccolithophores: From molecular processes to*  
651 *global impact*, Thierstein, H. R., & Young, J. R. (Eds.), Springer, 191-216.

652 Ziveri, P., Baumann, K.H., Böckel, B. Bollmann, J. and Young, J. (2004) Present day  
653 coccolithophore-biogeography in the Atlantic Ocean in Thierstein, H. and Young, J.

654 Eds. *Coccolithophores: From Molecular Processes to Global Impact*. Springer Verlag:  
655 403-428.

656 Ziveri, P., De Bernardi, B., Baumann, K.-H., Stoll, H. M., and Mortyn, P. G.: Sinking of  
657 coccolith carbonate and potential contribution to organic carbon ballasting in the deep  
658 ocean, *Deep-Sea Res. Pt. II*, 54, 659–675, <https://doi.org/10.1016/j.dsr2.2007.01.006>,  
659 2007.

660 Ziveri, P., Gray, W. R., Anglada-Ortiz, G., Manno, C., Grelaud, M., Incarbona, A., Rae,  
661 J. W. B., Subhas, A. V., Pallacks, S., White, A., Adkins, J. F., & Berelson, W. (2023).  
662 Pelagic calcium carbonate production and shallow dissolution in the North Pacific  
663 Ocean. *Nature Communications*, 14(1), 805. <https://doi.org/10.1038/s41467-023-36177->  
664 w

665 Ziveri, P., Passaro, M., Incarbona, A., Milazzo, M., Rodolfo-Metalpa, R., & Hall-  
666 Spencer, J. M. (2014). Decline in Coccolithophore Diversity and Impact on Coccolith  
667 Morphogenesis Along a Natural CO<sub>2</sub> Gradient. *The Biological Bulletin*, 226(3), 282–  
668 290. <https://doi.org/10.1086/BBLv226n3p282>

669

670

**Fig 1**

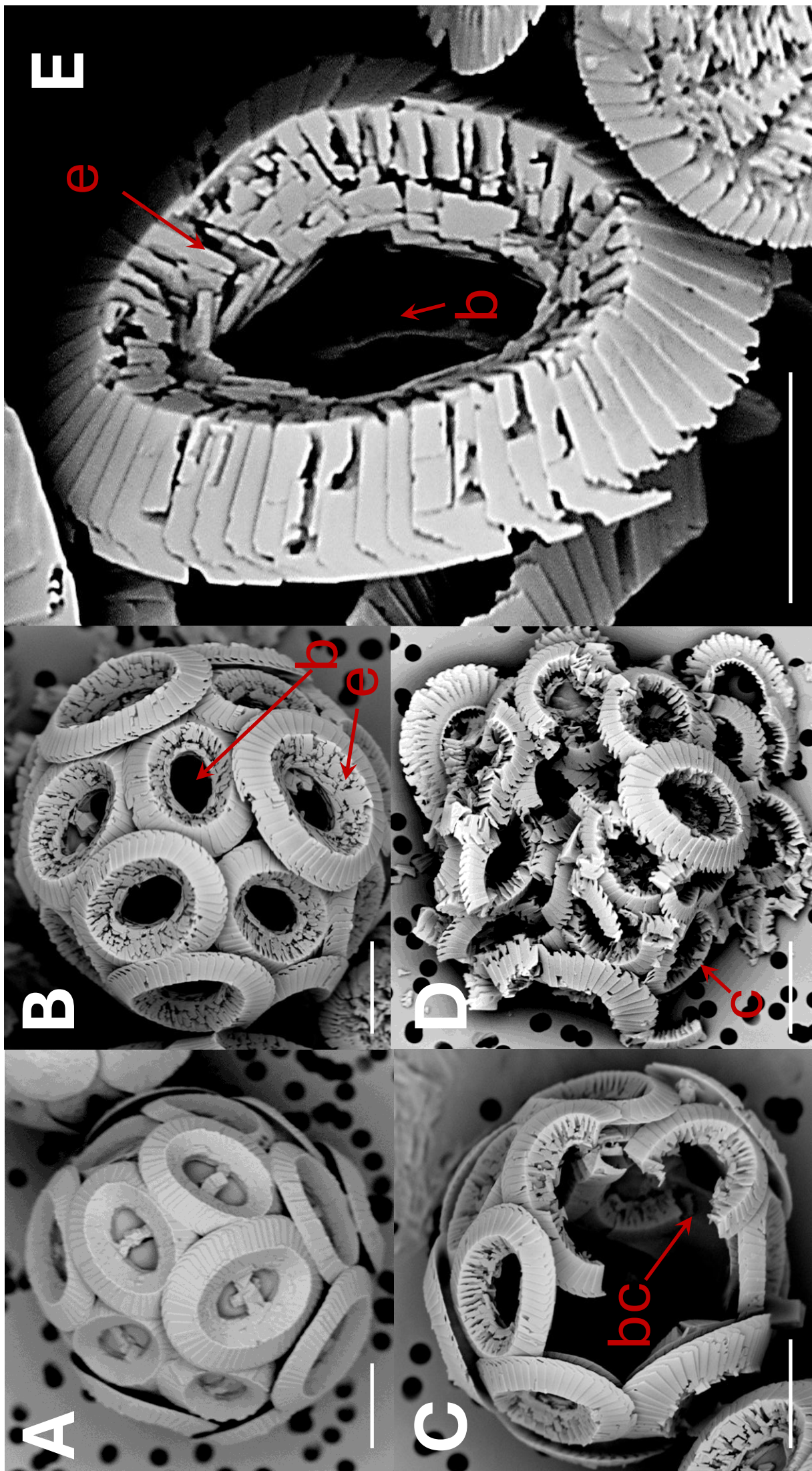


Fig 1 *Coccolithus braarudii*

A) coccosphere at  $t_0$ , no dissolution. Scale bar  $5\mu\text{m}$ . B) coccosphere; etching (e) of tube and distal shield and central area bar missing (b). Scale bar  $5\mu\text{m}$ . C) broken coccoliths (bc), etching of tube, central bar missing and gaps in coccosphere. Scale bar  $5\mu\text{m}$ . D) collapsed coccosphere (c), also showing etching (e) of tube and distal shield and central area bar missing (b). Scale bar  $5\mu\text{m}$ . E) coccolith, etching (e) of tube and distal shield, and central area bar missing (b). Note that the etching consistently occurs by opening of sutures between elements rather than by dissolution of element surfaces. Scale bar  $3\mu\text{m}$ .

**Fig 2**

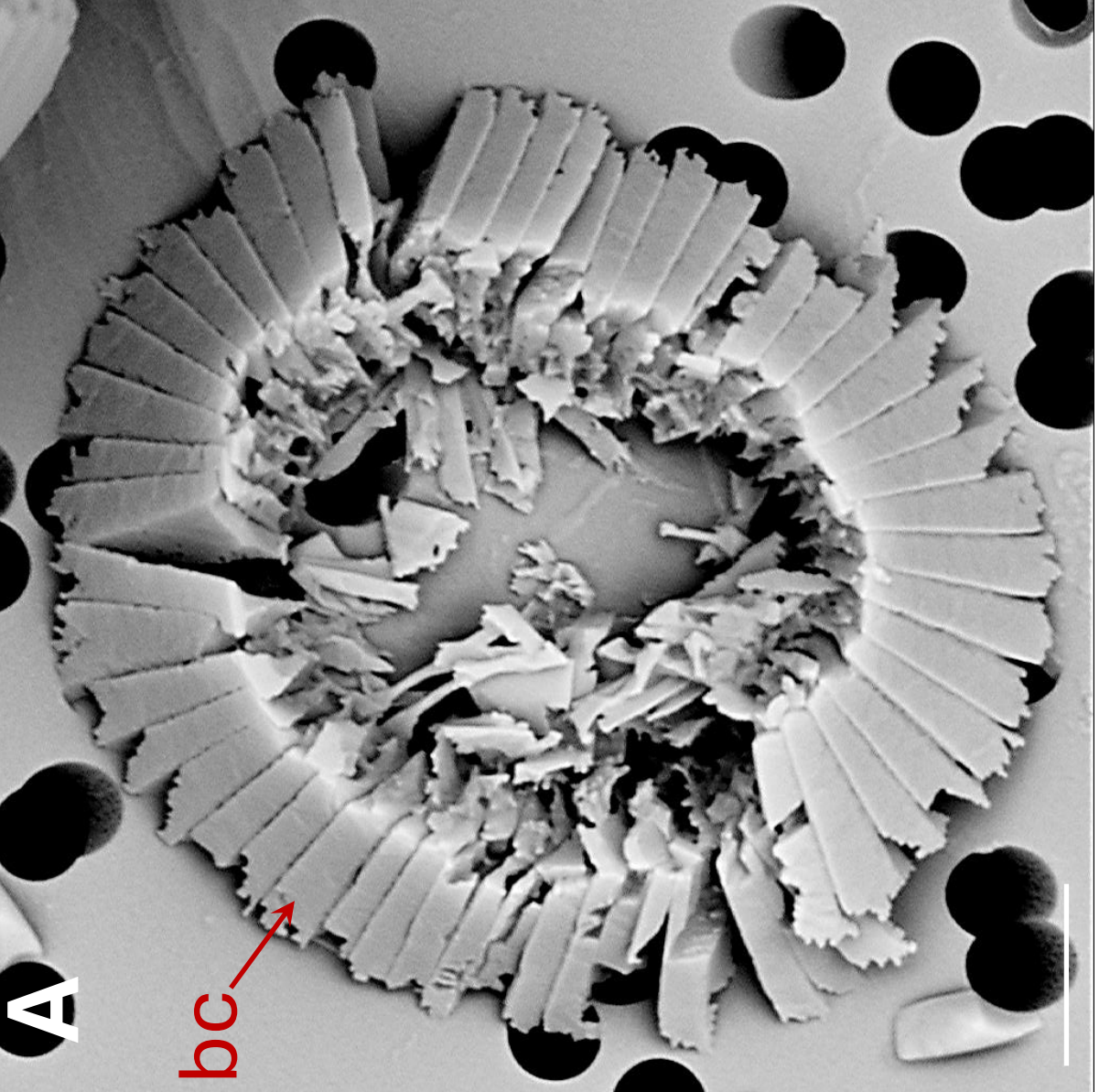
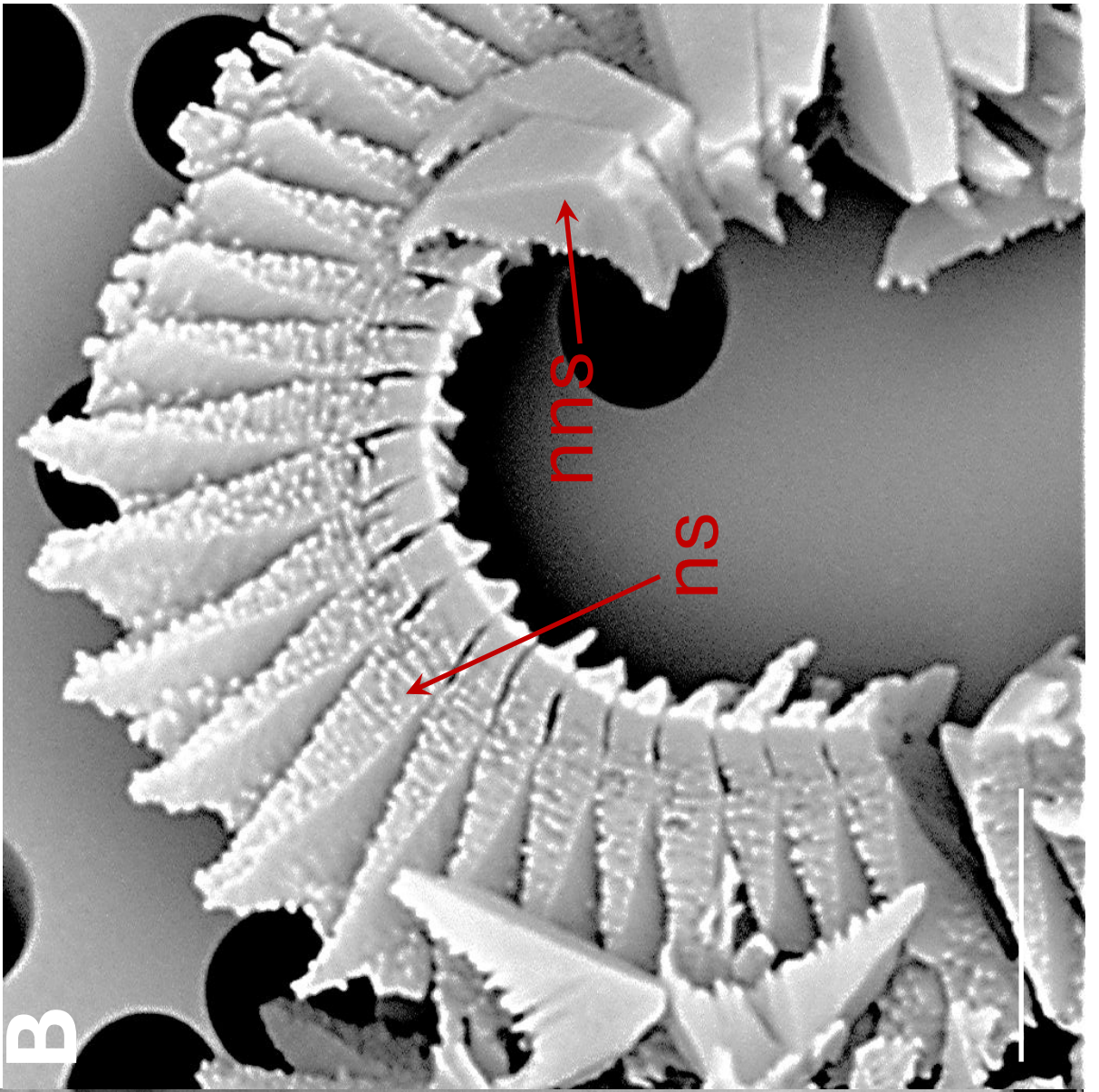


Fig 2 *Coccolithus braarudii*

A) broken coccolith (bc) distal shield in distal view. B) broken coccolith proximal view of distal shield showing nanostructure (ns); the arrow indicates isolated distal shield elements in distal view, from another coccolith, not displaying nanostructure (nns) on distal and vertical surfaces. All scale bars 2 $\mu$ m.

**Fig 3**

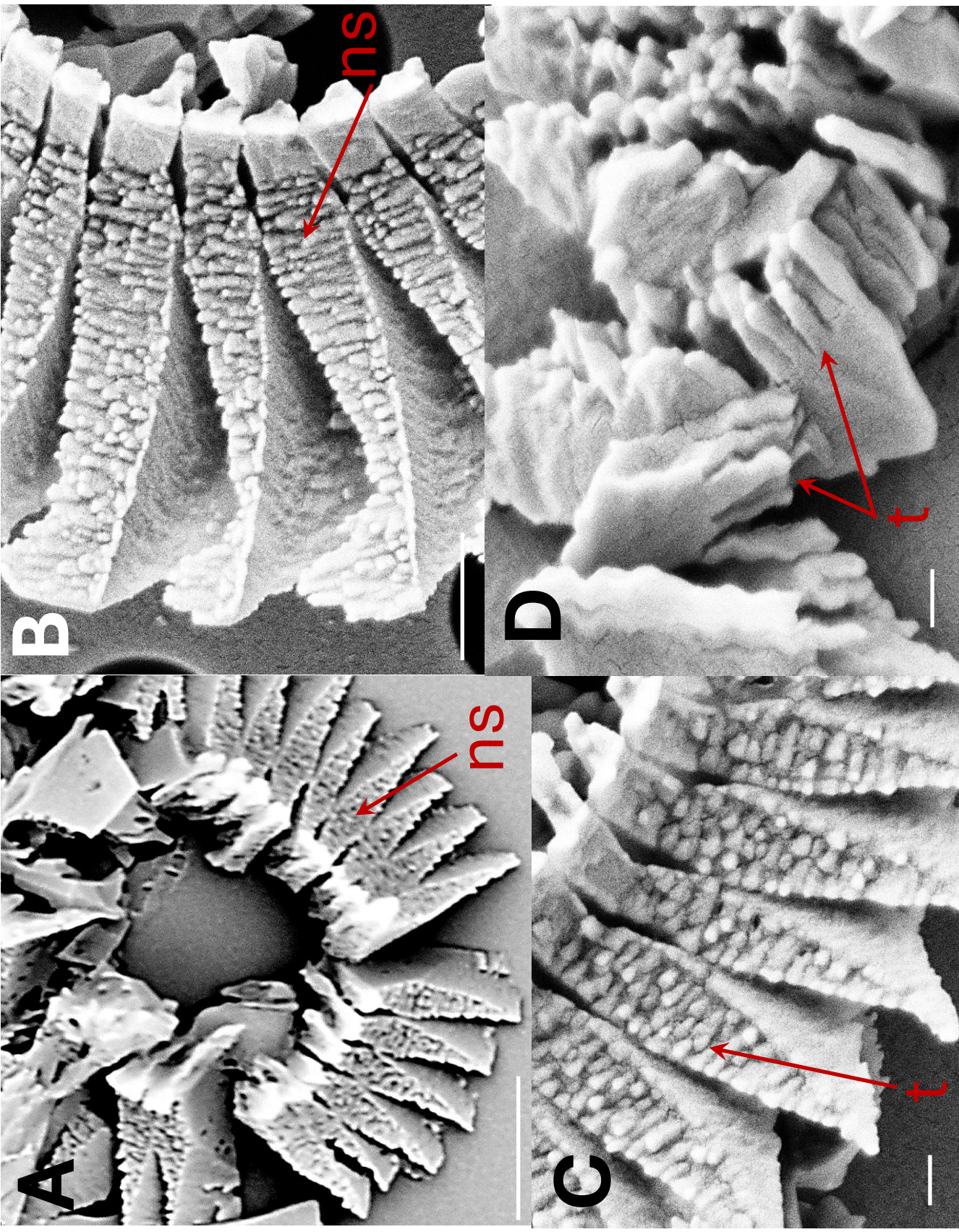


Fig 3 *Coccolithus braarudii*

A) broken coccolith distal shield in proximal view showing nanostructure (ns). Scale bar 2 $\mu$ m B) proximal view of distal shield elements showing nanostructure (ns). Scale bar 500nm. C) proximal view of distal shield elements showing nanostructure (ns); individual "tubercles" (t) of the nanostructure are ca 50-100nm, Scale bar 200nm. D) isolated distal shield elements showing nanostructure "tubercles" (t) in vertical side view (arrow). Scale bar 200nm.

**Fig 4**

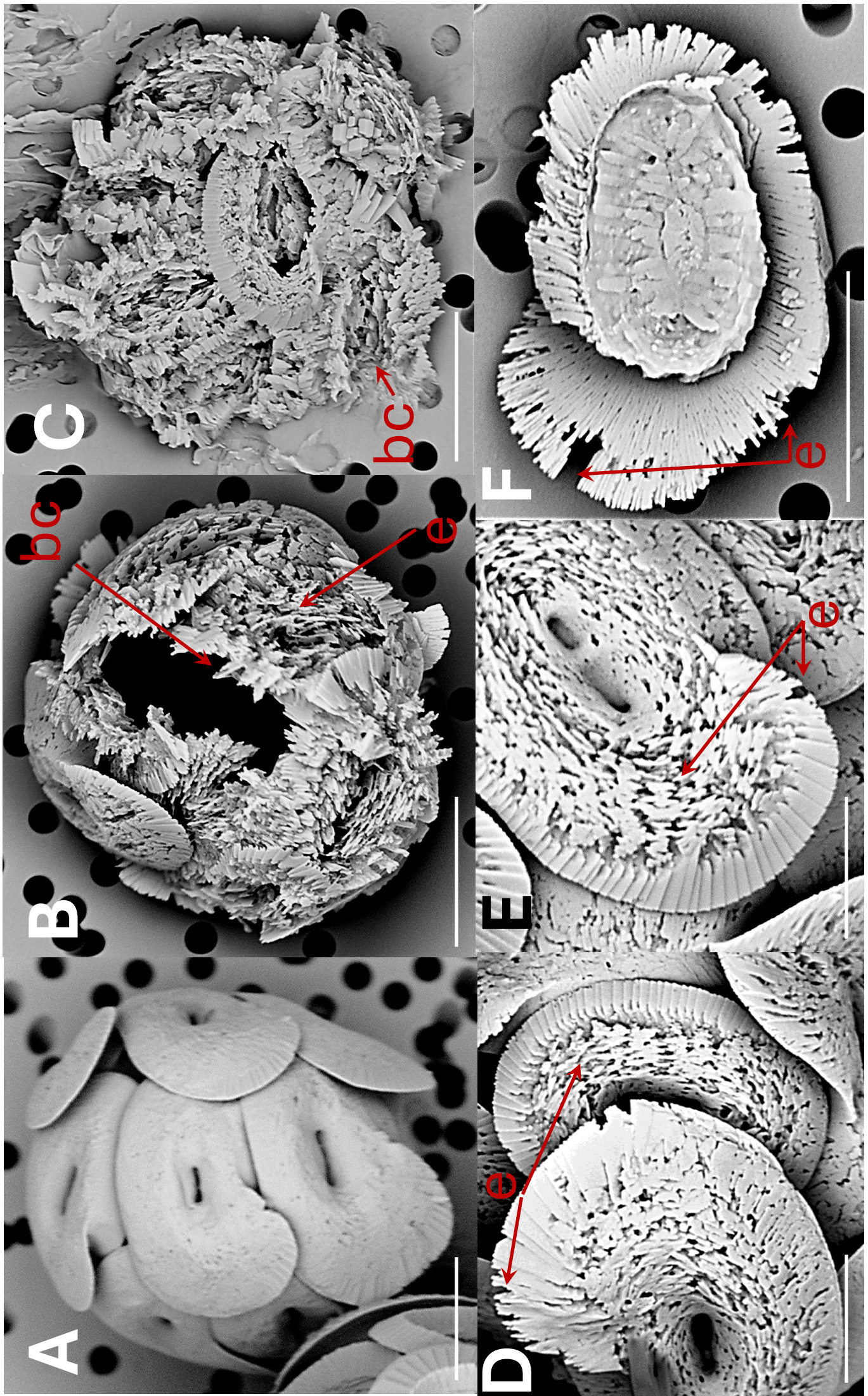


Fig 4 *Helicosphaera carteri*

A) coccosphere at t0, no dissolution. Scale bar 5 $\mu$ m. B) coccosphere displaying coccoliths with severe etching (e) and a broken coccolith (bc). Scale bar 5 $\mu$ m. C) collapsed coccosphere including broken coccoliths (bc). Scale bar 5 $\mu$ m. D) coccoliths in distal view with etching (e) in flange and blanket. Scale bar 3 $\mu$ m. E) coccolith in distal view with etching in flange and blanket. Scale bar 2 $\mu$ m. F) coccolith in proximal view with etching (e) in flange. Scale bar 5 $\mu$ m.

**Fig 5**

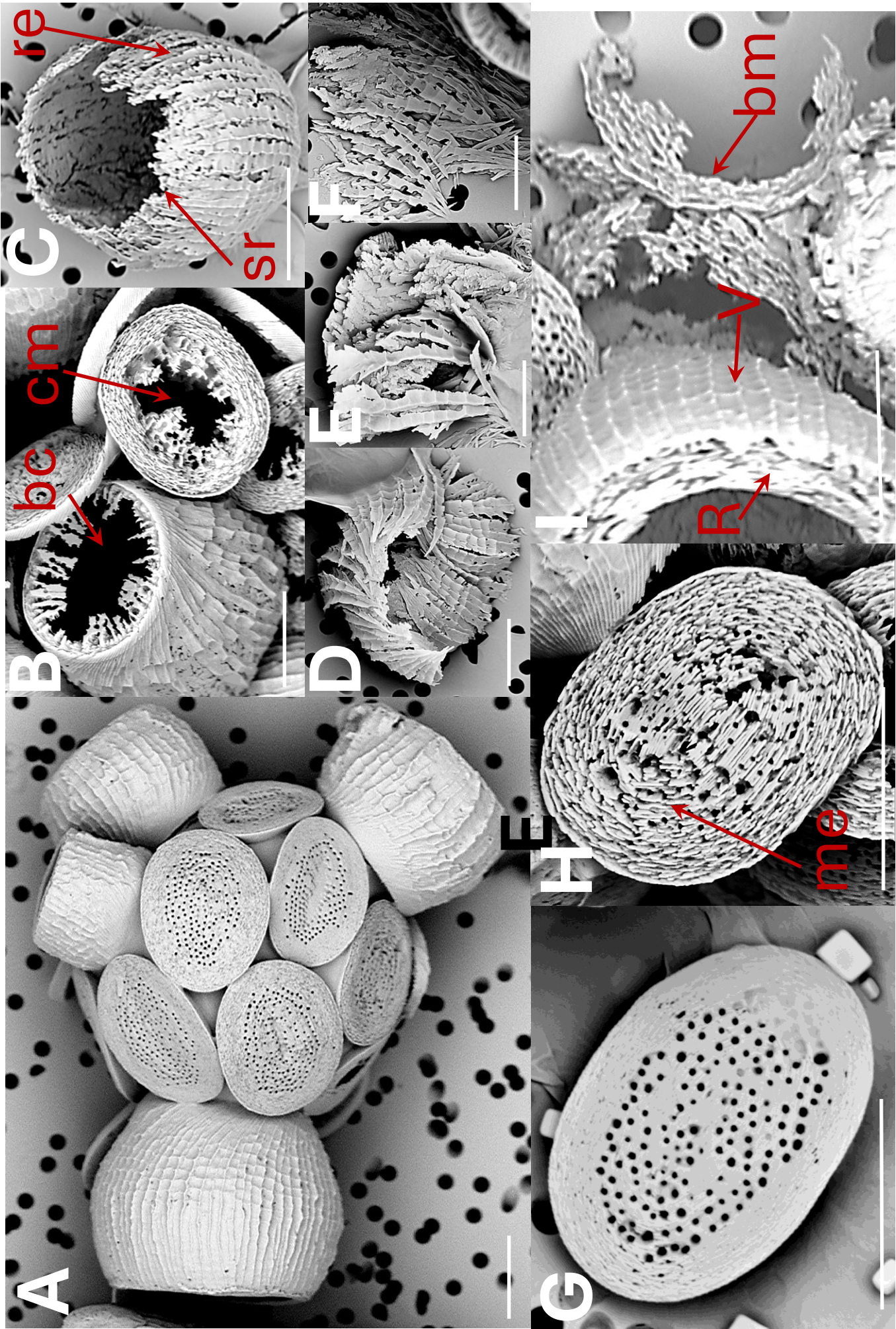
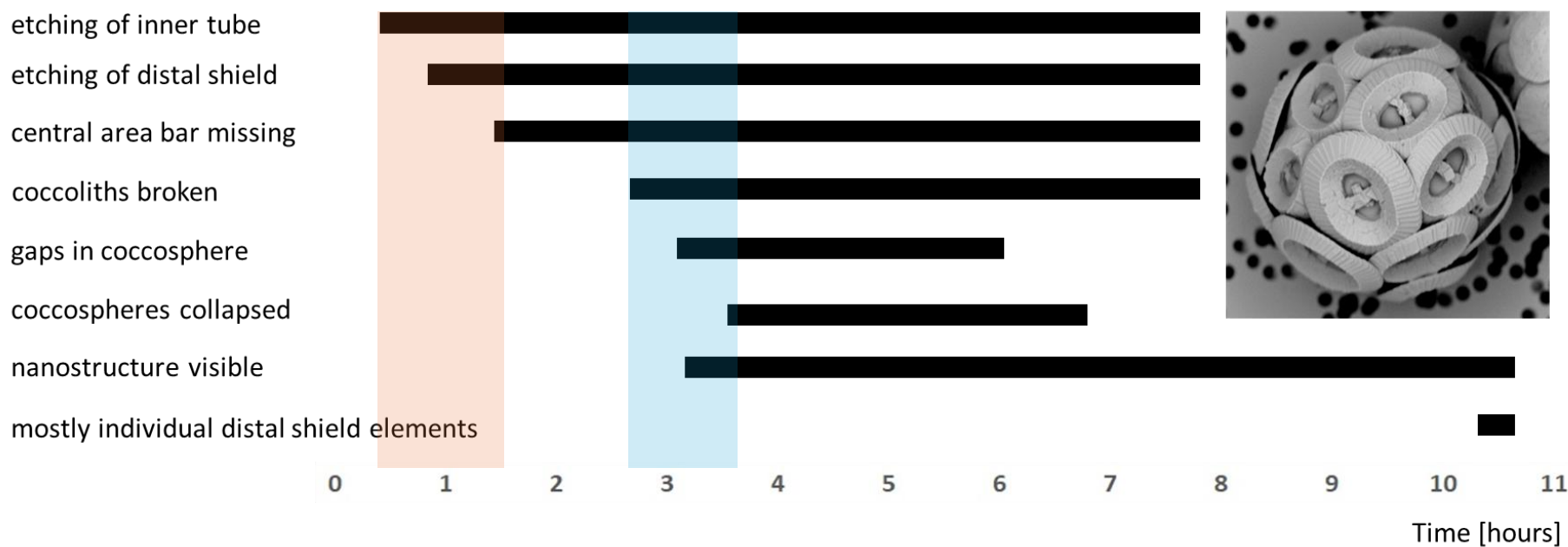


Fig 5 *Scyphosphaera apsteinii*

A) coccosphere at t0, no dissolution B) lopadolith base etching (be);  
murolith centre missing (cm) C) lopadolith barrel etching (re) and  
serrated rim (sr) D and E) broken lopadoliths F) isolated V-units G)  
murolith at t0, no dissolution H) murolith with etching (me) I)  
lopadolith in distal view showing R- and V-units (R- and V arrows,  
Young 2008); and broken murolith (bm). All scale bars 5 $\mu$ m.

Fig 6

***Coccolithus braarudii***



***Helicosphaera carteri***



***Scyphosphaera apsteinii***

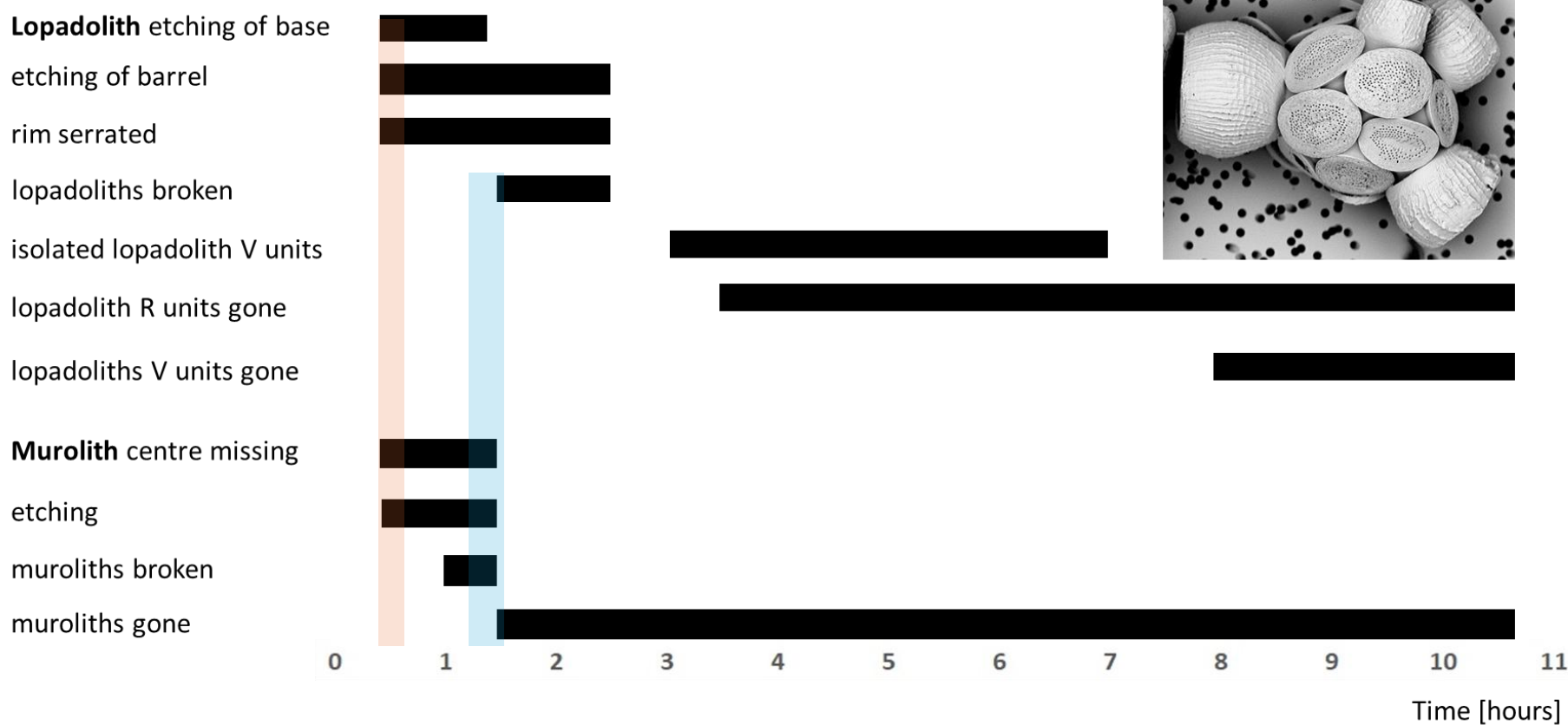


Fig 6 Timelines of dissolution. Bars indicate the period during which the respective feature can be observed. Shaded backgrounds indicate the onset points of major features. Pink backgrounds indicate the onset of etching, blue backgrounds indicate the onset of breakage/collapse. For example-images of each feature see Figs 1-5.

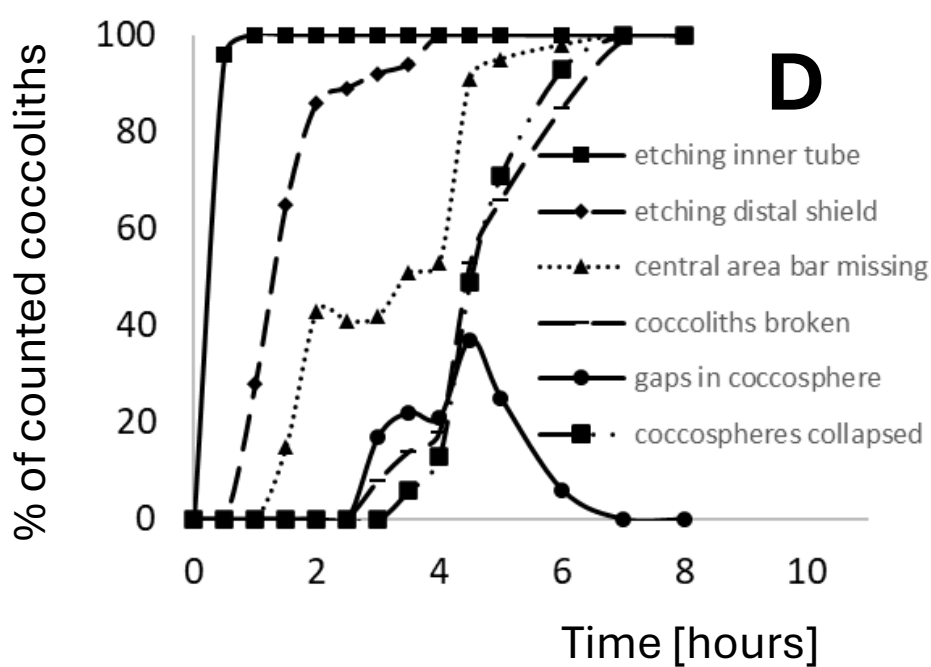
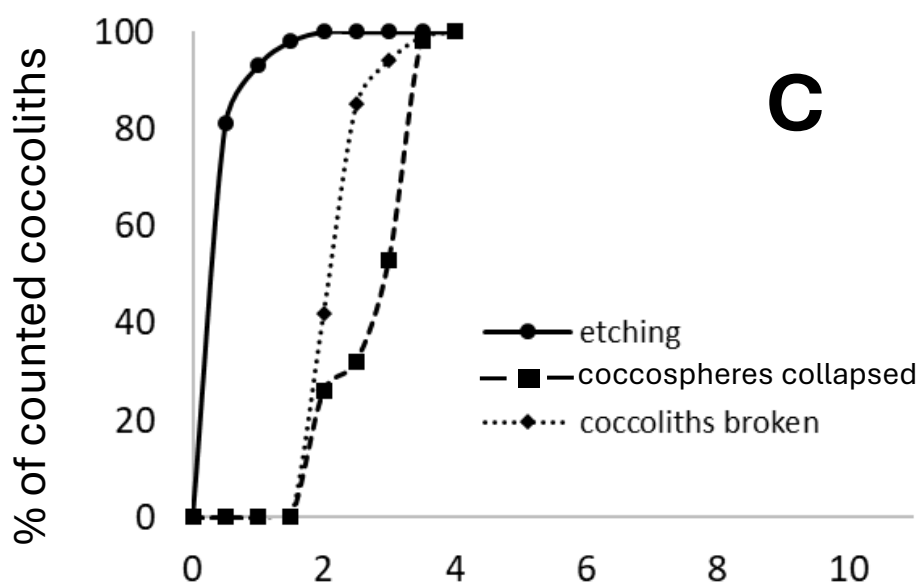
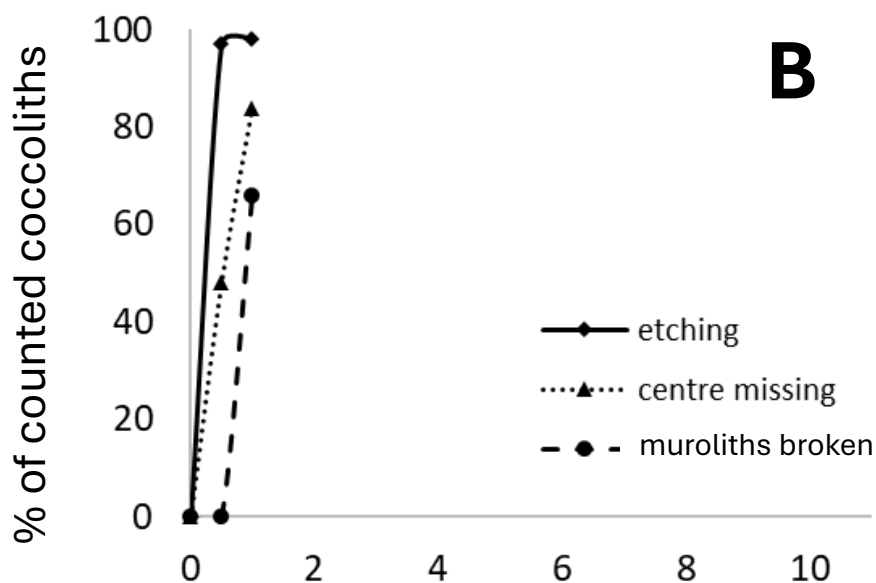
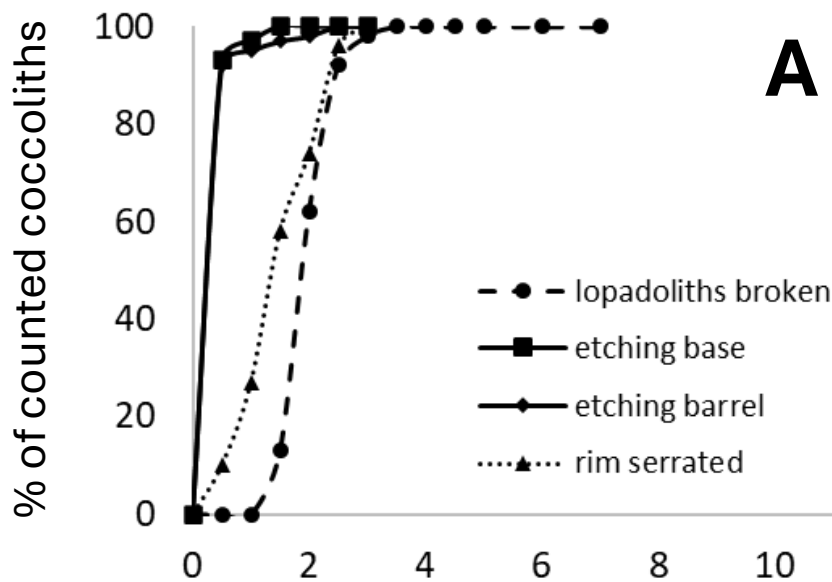


Fig 7 Quantification of the observations illustrated in Fig 6. Plotted is the percentage of each analysed feature versus time in hours from start of experiment. A) *Scyphosphaera apsteinii* lopadoliths B) *Scyphosphaera apsteinii* muraliths C) *Helicosphaera carteri* D) *Coccolithus braarudii*

**Fig 8**

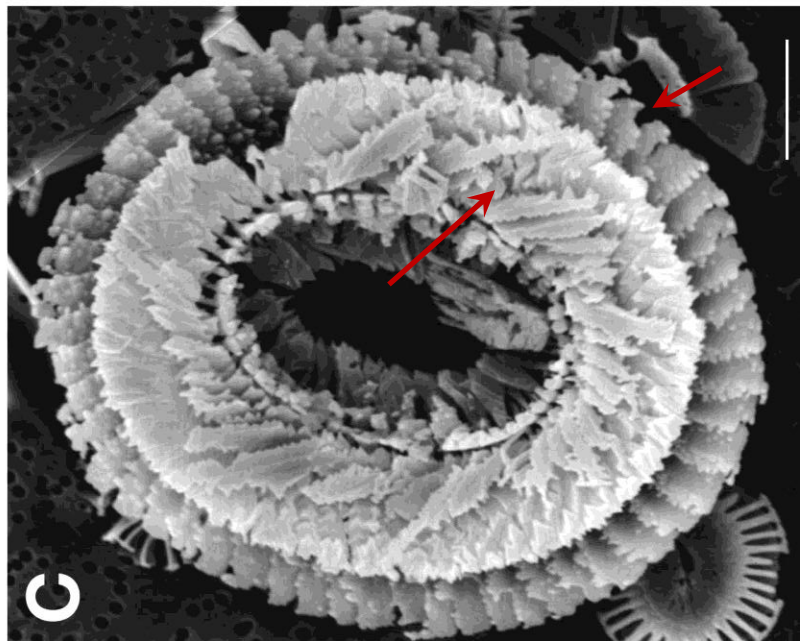
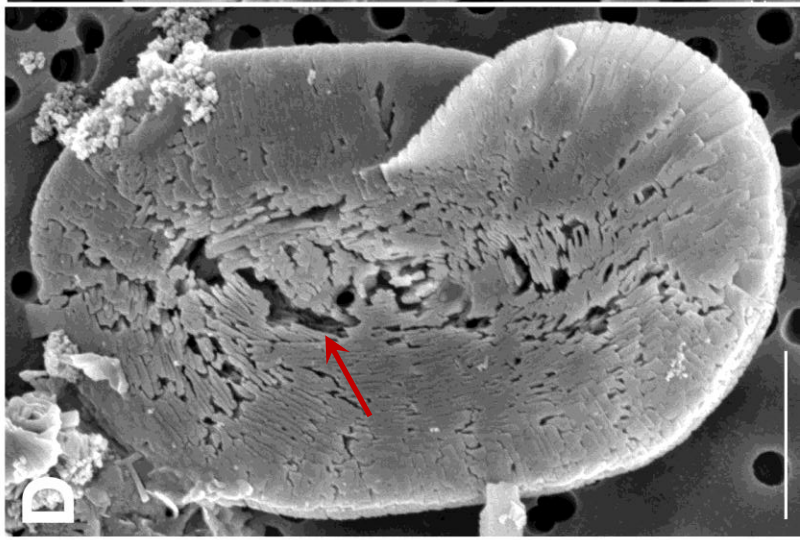
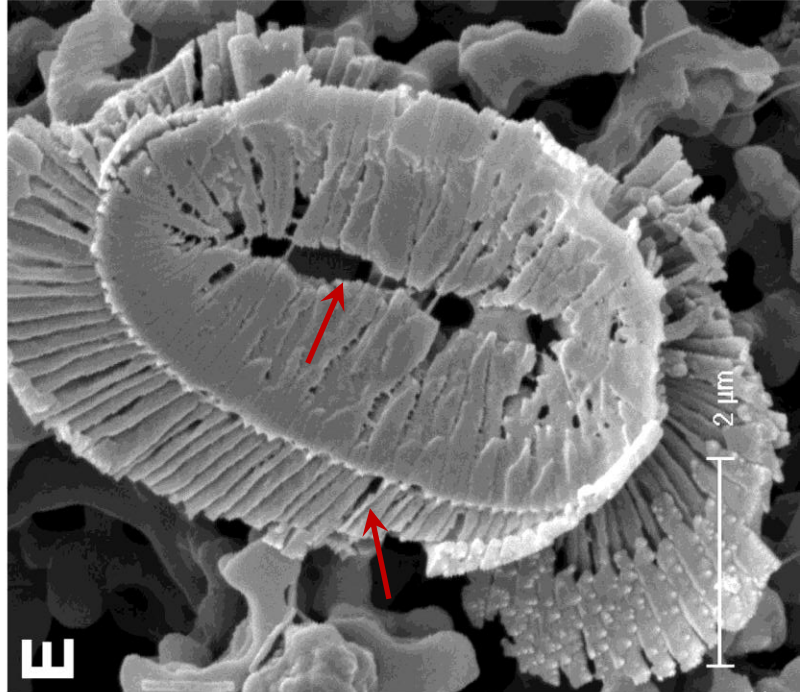


Fig 8 Field samples showing etching patterns comparable to those seen in the experimental samples (arrows). All scale bars 2  $\mu\text{m}$ .

*Coccolithus braarudii*: A) Lower surface of a broken piece of distal shield showing nanostructure. B) Central area of distal shield showing early stage dissolution. C) Proximal surface showing advanced dissolution.

*Helicosphaera carteri*: D) Distal Surface showing early stage dissolution. E) Proximal surface showing advanced dissolution.

A, B - sediment trap samples from 3200m, N. Atlantic; C - surface water sample, NW Atlantic; D- sediment trap sample, Canaries, 200m; E plankton sample from 120m, Gulf of Mexico.